In-medium jet shape from energy collimation in parton showers: comparison with CMS PbPb data at 2.76 GeV

Redamy Perez Ramos, Thorsten Renk

In-medium jet shape from energy collimation in parton showers: comparison with CMS PbPb data at 2.76 GeV

Redamy Pérez-Ramos [1]

Department of Physics, P.O. Box 35, FI-40014 University of Jyväskylä, Finland

Thorsten Renk [2]

Department of Physics, P.O. Box 35, FI-40014 University of Jyväskylä, Finland,
Helsinki Institute of Physics, P.O. Box 64, FI-00014 University of Helsinki, Finland

Abstract: We present the medium-modified energy collimation and the jet shape in the leading-logarithmic approximation of QCD. As a consequence of more accurate kinematic considerations in the argument of the Dokshitzer-Gribov-Lipatov-Altarelli-Parisi (DGLAP) fragmentation functions (FFs) we find a correction of order $\mathcal{O}(\alpha_s)$ which accounts for the scaling violation of DGLAP FFs at small x. We also compare our calculations with the event generator YaJEM. The modification of jets by the medium in both cases is implemented by altering the infra-red sector using the Borghini-Wiedemann model. The energy collimation and jet shapes qualitatively describe a clear broadening of showers in the medium, which is further supported by YaJEM in the final comparison of the jet shape with CMS PbPb data at center of mass energy 2.76 GeV. The comparison of the biased versus unbiased YaJEM jet shape with the CMS data shows a more accurate agreement for biased showers and illustrates the importance of an accurate simulation of the experimental jet-Finding strategy.

[1] e-mail: redamy.r.perez-ramos@jyu.fi
[2] e-mail: trenk@phy.duke.edu

1 Introduction

The phenomenon of jet quenching has first been established experimentally through the observed suppression of high-p_T hadrons in nucleus-nucleus (A-A) collisions at the Relativistic Heavy Ion Collider (RHIC) and the Large Hadron Collider (LHC) [1–3]. It has then been confirmed by various other measurements that highly virtual partons produced in hard processes in a medium show modifications to the subsequent evolution of a QCD shower, in particular softening and broadening of the resulting hadron distribution which leads to a reduction in the yield of leading hadrons and jets [4–7].

In the vacuum, the production of highly virtual partons following the hard inelastic scattering of two partons from the incoming protons ($2 \to 2 + X$) is followed by the fragmentation into a spray of hadrons which are observed in high energy collider experiments. The evolution of successive splittings $q(\bar{q}) \to q(\bar{q})g$, $g \to gg$ and $g \to q\bar{q}$ (q, $\bar{q}$ and g label quark, anti-quark and gluon respectively) inside the parton shower prior to hadonization is well established and can be described by the DGLAP evolution equations for fragmentation functions in the leading logarithmic approximation (LLA) of QCD [8–10] or alternatively in terms of Monte-Carlo (MC) formulations such as the PYSHOW algorithm [11, 12]. In A-A collisions, partons produced in the hard inelastic scattering of two partons from nuclei ($2 \to 2 + X$) propagate through the hot/dense QCD media also produced in such collisions and their branching pattern is changed by interacting with the color charges of the deconfined QGP [13]. As a consequence, additional medium-induced soft gluon radiation is produced in A-A collisions, which leads for instance to jet broadening. At RHIC, the main observables considered to probe this physics were the nuclear suppression factor of single inclusive hadrons R_{AA} [14, 15] and the suppression factor of hard back-to-back dihadron correlations I_{AA} [16, 17].

In this paper, we aim at discussing two different observables currently relevant mainly for LHC physics: the energy collimation and the jet shape of medium-modified showers. We use a QCD-inspired model introduced by Borghini and Wiedemann (BW) [18] for the modification of the FFs by the medium where the medium evolution itself is described by a hydrodynamical evolution. In the BW model, the DGLAP splitting functions are enhanced in the infra-red sector in order to mimic the medium-induced soft gluon radiation. In practice, the $1/z$-dependence of the QCD vacuum splitting functions corresponding to the parton branchings $q(\bar{q}) \to q(\bar{q})g$ and $g \to gg$ are altered by introducing a parameter $N_{\rm s} = 1 + f_{med}$ ($f_{med} \geq 0$) in the form $P_{a\to bc}(z) = N_s/z + \mathcal{O}(1)$.

In the following we start with the quantification of the jet energy collimation and a study of the jet broadening in gluon and quark jets in LLA. The computation of the energy collimation was first performed analytically in the vacuum [19] and subsequently modeled in the medium [20] by mean of the inclusive spectrum of partons provided by the medium-modified solution of DGLAP FFs at large $x \sim 1$. For this purpose, a high energy jet of half opening angle Θ_0, energy E and virtuality $Q = E\Theta_0$ produced in a nucleus-nucleus collision was considered, followed by the production of one concentric sub-jet of opening angle Θ and transverse momentum $k_\perp = xE\Theta$ where the bulk $xE \sim E$ of the jet energy is contained [19, 20]. By definition, the smaller is the angle Θ where the jet energy is concentrated, the higher is the jet energy collimation [19]. The half opening angle of the jet Θ_0 should be fixed according to the jet definition used by the experiment. The energy collimation can be then determined by maximizing the

distribution of partons $D(x, E\Theta_0, E\Theta)$, which dominates the hard fragmentation ($x \sim 1$) of the jet into a sub-jet, as discussed in [20].

In this paper, we will provide a more accurate description of the energy collimation, which accounts for the x-dependence in the third argument of the FFs $D(x, \ln E\Theta_0, \ln xE\Theta)$. The account of the shift in $\ln x$ leads to a small next-to-LLA (NLLA) correction of order $\mathcal{O}(\alpha_s)$ which decreases the energy collimation at intermediate values of x as a consequence of the scaling violation of DGLAP FFs. We also compare the final energy collimation in NLLA with the medium-modified energy collimation extracted from the event generator YaJEM [21].

The integrated jet shape $\Psi(\Theta; \Theta_0)$ provides indeed an analogous measurement of how widely the energy of the jet is spread. This observable was first studied in the vacuum in [22] and generalized to the medium throughout the calculations presented in [23] in the framework of the cone and k_t jet reconstruction algorithms. By definition, $\Psi(\Theta; \Theta_0)$ determines the energy fraction ($x \equiv \Psi(\Theta; \Theta_0)$) of a jet of half opening angle Θ_0 that falls into a sub-jet of half opening angle Θ for a fixed jet energy E. In our framework, we extract the angular dependence of the sub-jet energy fraction from the simple prescription provided by the LLA energy collimation $x = f(E\Theta_0, E\Theta)$ at fixed energy E. In the comparison with MC, we do the jet shape analysis with Pythia 6 and YaJEM using the FastJet package on the events and compare our results with CMS pp and PbPb data for central collisions (0-10%) at 2.76 TeV [7].

Finally, for the purpose of a detailed comparison with data by the CMS experiment, the jet shape analysis with YaJEM is performed for both PbPb and pp collisions following the CMS analysis procedure closely. Jets are reconstructed with the anti-k_T algorithm [24, 25] with a resolution parameter $R(\equiv \Theta_0) = 0.3$. The clustering analysis is limited to charged particles with $e_i > 1$ GeV inside the jet cone where $E_{rec} \geq 100$ GeV is required for a jet (i.e. E_{rec} stands for the recovered jet energy inside the cone) [7]. The condition $e_i > 1$ GeV removes the soft QCD medium background which may blur the jet fragmentation and jet shape analysis. In order to illustrate the role of the bias caused by the jet finding procedure outlined above, we compare the biased jet shape (i.e. provided the CMS jet finding conditions are fulfilled) with an unbiased jet shape (which is a purely theoretical quantity) for both PbPb and pp CMS data.

2 Theoretical framework

2.1 Description of the process and kinematics

In Fig. 1, we consider the production of one gluon or quark ($A = g, q, \bar{q}$) jet of total energy E and opening angle Θ_0 which fragments into a sub-jet B of energy xE and opening angle Θ ($\Theta \leq \Theta_0$), where x is the energy fraction of A carried by B.

By definition, the virtualities of the jet A and the sub-jet B are $Q = E\Theta_0$ and $k_\perp = E_p\Theta$ ($E_p = xE$) respectively. The virtuality, also known as hardness of the jet, determines the phase space for radiation and hence sets the maximal transverse momentum of a parton inside the jet: $k_\perp \leq Q$. A minimal cut-off parameter Q_0 can be introduced $k_\perp \geq Q_0$, such that the minimal angle reached by a parton

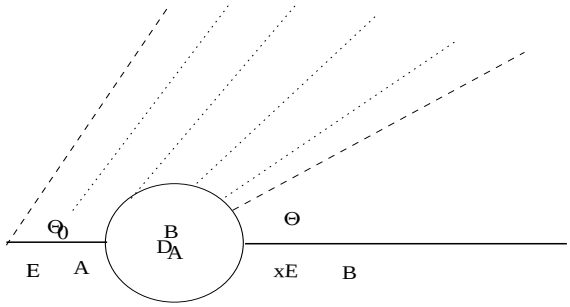

Figure 1: Fragmentation a jet A of half opening angle Θ_0 into a sub-jet B of half opening angle $\Theta < \Theta_0$.

inside the cascade equals $\Theta_{min} \geq Q_0/xE\Theta_0$. Experimentally, this physical picture corresponds to the calorimetric measurement of the energy flux deposited within a given solid angle. From the partonic point of view, the successive decays of partons in the cascade are ordered in $k_{\perp,i}$, or angles Θ_i due to the LLA kinematics for hard parton decays ($x \sim 1$) or due to the QCD coherence for soft parton decays ($x \ll 1$) [19]. Hard parton decays determine the bulk of the jet energy and are ruled by the LLA kinematics, which leads to DGLAP evolution equations [26], while soft parton decays determine the bulk of the jet multiplicity and are ruled by QCD coherence, which leads instead to the Modified-LLA (MLLA) evolution equations [19].

The jet energy collimation is characterized by the large energy fraction x of the sub-jet where the bulk of the jet energy inside the given cone $\Theta < \Theta_0 \ll 1$ is deposited. Hence, the probability for the energy fraction x to be deposited in a cone of aperture Θ is related to the DGLAP inclusive spectrum of partons through the formula [27],

$$D_A(x, E\Theta_0, xE\Theta) = \sum_{B=g,q} D_A^B(x, E\Theta_0, xE\Theta), \tag{1}$$

where the nature of partons B is not identified. In (1), the FFs $D_A^B(x, E\Theta_0, xE\Theta)$ determine the probability that a parton A produced at large $p_T \sim E$ in a high energy collision fragments into a hard sub-jet B of transverse momentum $xE\Theta$, which we write in the third argument of the FF. Qualitatively, (1) describes the evolution of the jet A in the $k_\perp$-range $xE\Theta \leq k_\perp \leq E\Theta_0$ according to the LLA $k_\perp$-ordering and hence, it determines the partonic skeleton of the sub-jet B before the hadronization takes place.

As compared to the FF for the inclusive spectrum of partons where the third argument is set to $E\Theta$ for hard partons $x \sim 1$: $D_A^B(x, E\Theta_0, E\Theta)$ [20], the formula (1) accounts for the energy fraction x of the sub-jet B in the FFs $D_A^B(x, E\Theta_0, xE\Theta)$. We can not compute $D_A^B(x, E\Theta_0, xE\Theta)$ by using DGLAP evolution equations because of the x-dependence included in the third argument, but we can instead expand it in powers of "$\ln x$" through the exponential operator:

$$D_A^B(x, E\Theta_0, xE\Theta) = e^{\ln x(\partial/\partial \ln(E\Theta))} D_A^B(x, E\Theta_0, E\Theta) \tag{2}$$

such that,

$$D_A^B(x, E\Theta_0, xE\Theta) = D_A^B(x, \Delta\xi) - \ln x \frac{\alpha_s(E\Theta_0)}{2\pi} e^{4N_c\beta_0\Delta\xi} \frac{\partial D_A^B}{\partial \Delta\xi}(x, \Delta\xi) + \mathcal{O}(\alpha_s^2), \tag{3}$$

where,

$$\xi(E\Theta) = \frac{1}{4N_c\beta_0}\ln\left[\ln\left(\frac{E\Theta}{\Lambda_{\rm QCD}}\right)^2\right], \quad \Delta\xi = \xi(E\Theta_0) - \xi(E\Theta), \quad \alpha_s(E\Theta_0) = \frac{2\pi}{4N_c\beta_0\ln\left(\frac{E\Theta_0}{\Lambda_{\rm QCD}}\right)}. \tag{4}$$

Hence, (1) can be rewritten in the form,

$$D_A(x, E\Theta_0, xE\Theta) = \sum_{B=g,q}\left[D_A^B(x,\Delta\xi) - \ln x\frac{\alpha_s(E\Theta_0)}{2\pi}e^{4N_c\beta_0\Delta\xi}\frac{\partial D_A^B}{\partial\Delta\xi}(x,\Delta\xi)\right] + \mathcal{O}(\alpha_s^2), \tag{5}$$

where α_s is the QCD coupling constant, β_0 is the first coefficient of the QCD β-function given by $\beta_0 = \frac{1}{4N_c}\left(\frac{11}{3}N_c - \frac{4}{3}T_R n_f\right)$, with $N_c = 3$, $T_R = \frac{1}{2}$, $n_f = 3$ and $\Lambda_{\rm QCD}(= 300)$ MeV is the mass scale of QCD. The new correction $\mathcal{O}(\alpha_s)$ is very small as $x \to 1$ and can be much larger for $x \approx 0.5$. As displayed in Fig. 1, the ladder Feynman diagrams leading to DGLAP evolution equations for $D_A^B(x,\Delta\xi)$ should be iterated from the hardest virtuality $Q = E\Theta_0$ of the process to the lower sub-jet virtuality $k_\perp = E\Theta$ through the variable $\Delta\xi$ in (4). Thus, $D_A^B(x,\Delta\xi)$ describes the distribution of partons B with transverse momentum $k_\perp = E\Theta$ contained inside the parton A, which fixes the initial scale of the hard process: $Q = E\Theta_0$; i.e. the virtuality. Therefore, we can estimate $D_A(x, E\Theta_0, xE\Theta)$ with the solution of DGLAP evolution equations for the FFs $D_A^B(x,\Delta\xi)$, which appear in the r.h.s. of (5).

2.2 Medium-modified DGLAP evolution equations with the BW model

The DGLAP evolution equations for the splitting $A[1] \to B[z]C[1-z]$ (where z is the energy fraction of one parton in the splitting) in the $k_\perp$-range $E\Theta \le k_\perp \le E\Theta_0$ takes the simple form [26]:

$$\frac{d}{d\ln E\Theta}D(x, E\Theta_0, E\Theta) = \frac{\alpha_s(E\Theta)}{4\pi}\int_x^1\frac{dz}{z}P(z)D\left(\frac{x}{z}, E\Theta_0, E\Theta\right), \tag{6}$$

where $P(z)$ is the evolution "Hamiltonian" given by the regularized splitting functions [8–10]. In order to account for the medium-induced soft gluon radiation in heavy-ion collisions, we make use of the QCD-inspired model proposed in [18] which leads to a simple solution of the evolution equations at $x \sim 1$. In this model, the infrared parts of the splitting functions are arbitrarily enhanced by the factor $N_s = 1 + f_{med}$, where $f_{med} \ge 0$ accounts for medium-induced soft gluon radiation. The medium-modified splitting functions in z-space are written in the form [18],

$$P_{gg}(z) = 4N_c\left[\frac{N_s}{z} + \left[\frac{N_s}{1-z}\right]_+ + z(1-z) - 2\right], \quad P_{gq}(z) = 2\,T_R[z^2 + (1-z)^2], \tag{7a}$$

$$P_{qg}(z) = 2\,C_F\left(\frac{2N_s}{z} + z - 2\right), \quad P_{qq}(z) = 2\,C_F\left(\left[\frac{2N_s}{1-z}\right]_+ - 1 - z\right), \tag{7b}$$

where the $[\dots]_+$ prescription defined as $\int_0^1 dx[F(x)]_+ g(x) \equiv \int_0^1 dx F(x)[g(x) - g(1)]$. The solutions of (6) can most conveniently be obtained in Mellin space $\mathcal{D}(j, E\Theta_0, E\Theta)$ through the transformation

$$\mathcal{D}(j, E\Theta_0, E\Theta) = \int_0^1 dx\, x^{j-1}D(x, E\Theta_0, E\Theta),$$

such that the convolution (6) yields,

$$\frac{d}{d\ln E\Theta}\mathcal{D}(j,E\Theta_0,E\Theta)=\mathcal{P}(j)\mathcal{D}(j,E\Theta_0,E\Theta),\quad \mathcal{P}(j)=\int_0^1 dz\, z^{j-1}P(z). \tag{8}$$

The advantage of the Mellin transform can be clearly seen in (8). The convolution over z in (6) reduces to the product of the Mellin transformed splitting functions $\mathcal{P}(j)$ and the FFs $\mathcal{D}(j,E\Theta_0,E\Theta)$. Making use of the variables introduced in (4), (8) can be more explicitly rewritten in the matrix form at LO:

$$\frac{d}{d\xi}\begin{pmatrix}\mathcal{D}_{q_{\rm NS}}(j,\xi)\\ \mathcal{D}_{q_{\rm S}}(j,\xi)\\ \mathcal{D}_g(j,\xi)\end{pmatrix}=\begin{pmatrix}\mathcal{P}_{qq}(j) & 0 & 0\\ 0 & \mathcal{P}_{qq}(j) & \mathcal{P}_{qg}(j)\\ 0 & \mathcal{P}_{gq}(j) & \mathcal{P}_{gg}(j)\end{pmatrix}\begin{pmatrix}\mathcal{D}_{q_{\rm NS}}(j,\xi)\\ \mathcal{D}_{q_{\rm S}}(j,\xi)\\ \mathcal{D}_g(j,\xi)\end{pmatrix}, \tag{9}$$

where $\mathcal{D}_{q_{\rm NS}}$ and $\mathcal{D}_{q_{\rm S}}$ stand respectively for the flavor non-singlet and flavor-singlet quark distributions, and $\mathcal{P}_{ik}(j)$ are the Mellin transforms of the LO splitting functions:

$$\begin{aligned}
\mathcal{P}_{gg}(j) &= -4N_c\left[N_s\,\psi(j+1)+N_s\gamma_E-\frac{N_s-1}{j}-\frac{N_s-1}{j-1}\right]\\
&\quad+\frac{11N_c}{3}-\frac{2n_f}{3}+\frac{8N_c(j^2+j+1)}{j(j^2-1)(j+2)}, &\text{(10a)}\\
\mathcal{P}_{gq}(j) &= T_R\,\frac{j^2+j+2}{j(j+1)(j+2)}, &\text{(10b)}\\
\mathcal{P}_{qg}(j) &= 2\,C_F\,\frac{(2N_s-1)(j^2+j)+2}{j(j^2-1)}, &\text{(10c)}\\
\mathcal{P}_{qq}(j) &= -C_F\left[4N_s\,\psi(j+1)+4N_s\gamma_E-4\frac{N_s-1}{j}-3-\frac{2}{j(j+1)}\right]. &\text{(10d)}
\end{aligned}$$

This method allows for the diagonalization of the "Hamiltonian" given by the set $\mathcal{P}(j)$ with respect to the "evolution-time" variable $\xi\sim t=\ln(E\Theta)$. In some limits at large and small x, analytical solutions of the equations can be found through this method [26] but for numerical computation, solving the equations directly in x-space turns out to be more efficient than inverting the Mellin transform numerically. Thus, at large energy fraction $x\sim 1$, or equivalently large $j\gg 1$ we are interested in, the expressions for the Mellin representation of the splitting functions (10a)-(10d) can be reduced to:

$$\mathcal{P}_{qq}(j)\approx 4C_FN_s\left(-\ln j+\frac{3}{4N_s}-\gamma_E\right),\quad \mathcal{P}_{gg}(j)\approx 4N_cN_s\left(-\ln j+\frac{\beta_0}{N_s}-\gamma_E\right), \tag{11}$$

where the asymptotic behavior of the digamma function $\psi(j+1)\approx\ln j$ is replaced at $j\gg 1$ [26]. The off-diagonal matrix elements vanish in this approximation: $\mathcal{P}_{gq}(j)=\mathcal{P}_{qg}(j)=0$.

Note that the $N_s\ln j$-dependence in (11) arises from the $[N_s/(1-z)]_+$ terms of the DGLAP splitting functions, such that for hard partons $z\sim 1$, the enhanced contribution of the soft $1-z\sim 0$ component $[1/(1-z)]_+$ originates the sub-jet broadening within this approximation. Qualitatively, as a consequence of energy conservation, if soft gluon radiation is enhanced in the region $\Theta\leq\Theta'\leq\Theta_0$ for a fixed jet energy E, the sub-jet energy (B, xE) should be smaller compared to its value in the vacuum and the energy collimation should then decrease, i.e. Θ should increase.

Going back to x-space requires to take the inverse Mellin transform given by

$$D(x,\Delta\xi)=\frac{1}{2\pi i}\int_C dj\, x^{-j}\mathcal{D}(j,\Delta\xi), \tag{12}$$

where the contour C in the complex plane is parallel to the imaginary axis and lies to the right of all singularities. Since we are interested in the large $j\gg 1$ ($x\sim 1$) approximation, we insert (11) into (9). After integrating what results, we get the medium-modified distribution at large $x\sim 1$,

$$D_A^A(x,\Delta\xi)\simeq(1-x)^{-1+4C_AN_s\Delta\xi}\,\frac{\exp[4C_AN_s(\frac{3}{4N_s}-\gamma_E)\Delta\xi]}{\Gamma(4C_AN_s\Delta\xi)}. \tag{13}$$

where β_0 is replaced by $3/4$ ($n_f=3$) in (11). The corresponding result in the vacuum for $N_s=1$ is given in [26].

Within this approximation, the parton initiating the jet A is identical to that initiating the sub-jet $B=A$, $C_A=N_c$ if A is a gluon and $C_A=C_F=\frac{4}{3}$ if A is a quark. Indeed, the FF $D_A^A(x,\Delta\xi)$ in (13) describes the splittings $g\to gg$ and $q\to qg$ and as constructed, it neglects the others: $g\to q\bar{q}$ and $q\to gq$. Therefore, the sum over B in (5) disappears such that,

$$D_A^A(x,E\Theta_0,xE\Theta)=D_A^A(x,\Delta\xi)-\ln x\frac{\alpha_s(E\Theta_0)}{2\pi}e^{4N_c\beta_0\Delta\xi}\frac{\partial D_A^A}{\partial\Delta\xi}(x,\Delta\xi)+\mathcal{O}(\alpha_s^2). \tag{14}$$

In a more accurate solution of this problem which could only be achieved numerically, the whole sum of the parton branchings given by $D_q(x,E\Theta_0,xE\Theta)=D_q^q(x,E\Theta_0,xE\Theta)+D_q^g(x,E\Theta_0,xE\Theta)$ for a quark jet and $D_g(x,E\Theta_0,xE\Theta)=D_g^g(x,E\Theta_0,xE\Theta)+D_g^q(x,E\Theta_0,xE\Theta)$ for a gluon jet, with the full resummed contribution of the soft gluon/collinear logarithms arising from the N_s/z-dependence of the splitting functions in the FO approach of DGLAP FFs [28, 29].

2.3 Jet energy collimation

As discussed in [26], the distribution (13) presents a certain maximum at some angle Θ where the bulk of the jet energy is concentrated. The reason for this can be understood as follows: for $\Delta\xi\to 0$, or $\Theta\to\Theta_0$, almost the whole energy is contained inside the cone Θ_0 (i.e. $D\to\delta(1-x)$) and the probability distribution D_A^A for $x\neq 1$ should decrease. For Θ decreasing $\Theta\gg\Lambda_{\rm QCD}/E$ (notice that the x-dependence was reabsorbed on the pre-exponential term in (2)), the emission outside the cone Θ grows and the fragmentation probability decreases thereby. Then, taking the first derivative over $\ln\Theta$ in (14) leads to the NLLA equation for Θ:

$$\begin{aligned}&\left[\ln(1-x)+\frac{3}{4N_s}-\gamma_E-\psi(4C_AN_s\Delta\xi)\right]\left(1-4N_c\beta_0e^{b\Delta\xi}\ln x\frac{\alpha_s(E\Theta_0)}{2\pi}\right)=\\&4C_AN_se^{4N_c\beta_0\Delta\xi}\ln x\frac{\alpha_s(E\Theta_0)}{2\pi}\left[\ln(1-x)+\frac{3}{4N_s}-\gamma_E-\psi(4C_AN_s\Delta\xi)\right]^2\\&-4C_AN_se^{4N_c\beta_0\Delta\xi}\ln x\frac{\alpha_s(E\Theta_0)}{2\pi}\psi^{(1)}(4C_AN_s\Delta\xi),\end{aligned} \tag{15}$$

which is the main theoretical result of this section. We invert (15) numerically in order to get the NLLA jet energy collimation $\Theta(x,E)$. In (15), $\psi(x)$ is the digamma function and $\psi^{(1)}(x)=\frac{d\psi(x)}{dx}$,

the polygamma function of the first order. Note that this is one correction; a more complete set of corrections of the same order can be also added if, for instance, one considers the next-to-leading order (NLO) corrections [30] to the approached splitting functions (11) in a more cumbersome approach of this problem. However, this term goes beyond DGLAP and corresponds to the so-called scaling violation in DGLAP fragmentation functions [31]. In our framework, this correction slightly increases the available phase space from the hardest (B, $x \sim 1$) to slightly softer partons (B, $x \sim 0.5$) and is therefore expected to decrease the energy collimation or increase Θ at intermediate x. As expected for harder partons $\ln x \sim 0$, the above equation (15) reduces to the simple one [20],

$$\psi(4C_A N_s \Delta\xi) = \ln(1-x) + \frac{3}{4N_s} - \gamma_E. \tag{16}$$

Symbolically, the inversion of the NLLA (15) and LLA (16) can be written for quark ($A = q, \bar{q}$) and gluon ($A = g$) jets in the simple form,

$$\frac{\Theta_A}{\Theta_0} = \left(\frac{E\Theta_0}{\Lambda_{\rm QCD}}\right)^{-\gamma_A(x,N_s)}. \tag{17}$$

Setting $\ln x \to 0$ in (15), the LLA expression for $\gamma_A(x, N_s)$ was simply written in the form [20]:

$$\gamma_A(x, N_s) = 1 - \exp\left[-\frac{N_c\beta_0}{C_A N_s}\psi^{-1}\left(\ln(1-x) + \frac{3}{4N_s} - \gamma_E\right)\right], \tag{18}$$

where ψ^{-1} is the inverse of the digamma function. The exponent $\gamma_A(x, N_s)$ provides indeed the medium-modified slope of the energy collimation as a function of N_s for a fixed value of the sub-jet energy fraction x and can be obtained numerically from the NLLA equation (15). In table 1, we display the values of the NLLA and LLA slopes for the sub-jets of energy fractions $x = 0.5$ and $x = 0.8$. The new equation (15) cannot be rewritten like (17) but it can be solved numerically.

NLLA, LLA	$x = 0.5$	$x = 0.8$	NLLA, LLA	$x = 0.5$	$x = 0.8$
$\gamma_g(x, 1.4)$	0.37	0.26	$\gamma_g(x, 1)$	0.54	0.38
$\gamma_q(x, 1.4)$	0.67	0.50	$\gamma_q(x, 1)$	0.83	0.65

Table 1: NLLA and LLA values of the slope $\gamma_A(x, N_s)$ of the energy collimation for $N_s = 1.4$ (medium) and $N_s = 1$ (vacuum).

From table 1, one may wonder why the NLLA (15) and LLA (16) slopes of the energy collimation are the same. Indeed, the coupling constant does not depend on the jet energy only, but rather on the product $E\Theta \gg \Lambda_{\rm QCD}$ through the term $\ln x e^{4N_c\beta_0\Delta\xi}\alpha_s(E\Theta_0) \sim \ln x \alpha_s(E\Theta)$ in (15). As the jet energy E increases, the sub-jet cone Θ decreases inversely proportional and $\alpha_s(E\Theta)$ should remain roughly constant. Therefore, the NLLA and LLA curves of the jet energy collimation should stay approximately parallel to each other asymptotically.

We can see in both cases that the nuclear suppression parameter N_s decreases the slope of the energy collimation, which translates into increasing the rate of the jet broadening asymptotically. In both medium

and vacuum: $\gamma_q > \gamma_g$, which physically means that quark jets are more collimated than gluon jets. The same trends should be confirmed in the forthcoming analysis of the jet energy collimation with the event generator YaJEM.

3 Comparison with YaJEM and QGP hydrodynamics

In order to gauge the impact of the approximations made in deriving the results of the preceding section, we compare with results for jet energy collimation obtained in a MC formulation of the in-medium jet evolution. Within such a model, the parton initiating a jet A does not have to be identical to that initiating the subject B and hence the full set of splittings $g \to gg$ and $g \to q\overline{q}$ is available for a gluon jet. In addition, exact energy-momentum conservation at every splitting vertex is enforced.

In vacuum, the PYSHOW algorithm [11, 12] is a well-tested numerical implementation of QCD shower simulation. For comparison with our analytic results, we use the Borghini-Wiedemann prescription implemented within the in-medium shower code [32].

3.1 The in-medium shower generator YaJEM

YaJEM is based on the PYSHOW algorithm, to which it reduces in the limit of no medium effects. It simulates the evolution of a QCD shower as an iterated series of splittings of a parent into two daughter partons $a \to bc$ where the energy of the daughters are obtained as $E_b = zE_a$ and $E_c = (1-z)E_a$ and the virtuality of parent and daughters is ordered as $Q_a \gg Q_b, Q_c$. The decreasing hard virtuality scale of partons provides splitting by splitting the transverse phase space for radiation, and the perturbative QCD evolution terminates once the parton virtuality reach a lower value $Q_0 = 1$ GeV, at which point the subsequent evolution is considered to be non-perturbative hadronization.

The probability distribution to split at given z is given by the same QCD splitting kernels and (their medium modification in the BW prescription) which we have used above, i.e. Eqs. (7a, 7b), however in the explicit kinematics of the MC shower the singularities for $z \to 0$ or $z \to 1$ are outside of accessible phase space and no $[\dots]_+$ regularization procedure is needed.

We will refer to the implementation of the BW prescription for in-medium showers in the following as YaJEM+BW (note that this corresponds to the FMED scenario described in [32]). This is distinct from the default version of the code YaJEM, YaJEM-DE, which is tested against multiple observables at both RHIC and LHC (see e.g. [33–35]) and is based on an explicit exchange of energy and momentum between jet and medium rather than a modification of splitting probabilities.

For a straightforward benchmark comparison with analytic results, a value of f_{med} can be chosen, the parton shower be computed and stopped at partonic or evolved using the Lund model to the hadronic level, then clustered using the anti-k_T algorithm and properties like collimation or jet shapes can then be extracted.

In a MC treatment of the shower evolution, using a constant value of f_{med} to characterize the medium is not needed and in fact not realistic once a comparison with data is desired. Following the procedure

in [32], the value of f_{med} is determined event by event by embedding the hard process into a hydrodynamical medium [36] starting from a binary vertex which is at (x_0, y_0) and following an eikonal trajectory ζ through the medium evaluating the line integral

$$f_{med} = K_f \int d\zeta [\epsilon(\zeta)]^{3/4} (\cosh \rho(\zeta) - \sinh \rho(\zeta) \cos \psi). \tag{19}$$

where ϵ os the local energy density of the hydrodynamical medium, ρ the local flow rapidity and ψ the angle between flow and the direction of parton propagation. Events are then generated for a large number of random (x_0, y_0) sampled from the transverse overlap profile

$$P(x_0, y_0) = \frac{T_A(\mathbf{r_0} + \mathbf{b}/\mathbf{2}) T_A(\mathbf{r_0} - \mathbf{b}/\mathbf{2})}{T_{AA}(\mathbf{b})}, \tag{20}$$

where T_A is a nuclear thickness function $T_A(\mathbf{r}) = \int dz \rho_A(\mathbf{r}, z)$ obtained from the Woods-Saxon density $\rho_A(\mathbf{r}, z)$, and all observables are averaged over a sufficiently large number of events. This leaves a single dimensionful parameter K_f characterizing the strength of the coupling between parton and medium which is tuned to reproduce the measured nuclear suppression factor R_{AA} in central 200 GeV AuAu collisions (see [32]). In practice, this procedure leads to an $\langle f_{med} \rangle \approx 0.4$ which we will use in the analytical expressions when a comparison with data is intended.

3.2 Medium-modified jet energy collimation

In this section we compare our NLLA (15) and LLA [20] predictions for the energy collimation with YaJEM with YaJEM+BW. The analysis is carried out for gluon and quark jets independently and including all particles in an event, i.e. no detector effects are simulated in this section.

We generate thousands of gluon and quark dijets (i.e. back-to-back jets) for different fixed values of the center of mass energy $\sqrt{s}$ taken in the range $\sqrt{s} = 100 - 1200$ GeV. By doing so, we fix the energy of the leading initial parton to be $E_{lp} = \sqrt{s}/2$ for each member in the dijet. The values of E_{lp} are thus not selected as in the standard procedure by sampling the initial energy (or p_T) distribution of partons provided by PDFs [37], nPDFs [38] and the LO matrix elements of the partonic cross-section as we do later when comparing with data.

Dijets are then reconstructed by using the anti-k_t algorithm [24, 25] inside the cone radii $R = 1.0, 0.3$ (Θ_0), in agreement with the hard collinear approximation where the NLLA and LLA predictions should be tested. Reconstructed jets can be sorted by energy ($E_{jet,1} > E_{jet,2} > \ldots$) event-by-event such that the most energetic one can be randomly selected from its pair for the analysis. Note that the jet reconstruction radius coincides with the opening angle of the jet $\Theta_0 = R$ and $\Theta = r$ with that of the sub-jet. The cone R contains the reconstructed average energy flux (E_{rec}) of the jet A and r the energy flux of the sub-jet B (xE_{rec}), as illustrated in Fig.2.

The energy collimation can be then extracted from the angular distribution of the energy flux in $r < R$: $\frac{1}{N_{\rm jets}} \frac{d^2N}{dedr}$ for $r < R$ ($\Theta < \Theta_0$). The recovered jet energy $E_{\rm rec}$ can be obtained by integrating $\frac{1}{N_{\rm jets}} \frac{d^2N}{dedr}$

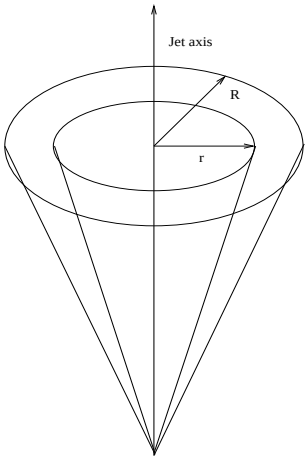

Figure 2: Jet ($\Theta_0 = R$) and sub-jet ($\Theta = r$) cones sharing the bulk of the jet energy.

over the whole range $0 < r \leq R$ such that the fraction x of the jet energy carried by the sub-jet $r < R$ can be written in the form:

$$x = \frac{1}{E_{\rm rec}} \int_0^r dr' \int de\, e \frac{d^2N}{dedr'}, \quad E_{\rm rec} = \int_0^R dr' \int de\, e \frac{d^2N}{dedr'}. \tag{21}$$

By fixing the energy fraction x in (21) to be large $x > 0.5$, we can numerically compute the sub-jet radius r where the bulk xE_{rec} of the reconstructed jet energy is contained. If the same procedure is repeated for different values of the center of mass energy $\sqrt{s}$, the energy evolution of the collimation $r(E_{\rm rec})$ can be then displayed as a function of $E_{\rm rec}$ for a fixed sub-jet energy fraction x.

The FastJet package [24, 25] provides the invariant mass $m_j = \sqrt{E_j^2 - \vec{p}_j^{\,2}}$ of each jet independently from its pair. The reconstructed virtuality of the jet inside small radii $R \ll 1$ can be related to the invariant mass of the dijet $M_{jj} \gg m_j$ through:

$$Q = \frac{M_{jj}}{2} R, \tag{22}$$

where M_{jj} can be expressed in terms of each m_j,

$$M_{jj}^2 = m_1^2 + m_2^2 + 2E_1E_2 - 2E_1E_2 \sqrt{\left(1 - \frac{m_1^2}{E_1^2}\right)\left(1 - \frac{m_2^2}{E_2^2}\right)} \cos\phi, \tag{23}$$

which should be evaluated with $m_1 \neq m_2$, $E_1 \neq E_2$ and $\phi \approx \pi$ for clustered back-to-back jets. Indeed, the jet finder misses part of the initial jet energy E_{lp} and invariant mass m_{lp} such that, the new values inside R are biased to smaller ones. Therefore, the reconstructed invariant mass of the dijet M_{jj} should be estimated as given in (23) for the biased E_i and m_i obtained with FastJet. The result in (22) can be checked to be in good agreement with the averaged one $Q = E_{rec}R$ displayed in the tables 2 and 3 in subsections 3.3 and 3.4 respectively; the smaller the R values, the more important is the bias and the better gets the agreement in the collinear limit, provided $R \geq \Lambda_{\rm QCD}/E_{rec}$. We rewrite (17) in the form,

$$r_A = R \left(\frac{Q}{\Lambda_{\rm QCD}}\right)^{-\gamma_A(x,N_s)}, \quad C_g = N_c = 3, \quad C_q = C_F = \frac{4}{3}, \tag{24}$$

for phenomenological treatment in gluon ($C_g = N_c$) and quark ($C_q = C_F$) jets with $r_A \leq R$. We choose $\Lambda_{\rm QCD} = 300$ MeV, the same value as in the PYSHOW showering algorithm and do not use the Lund model for the hadronization of partons into hadrons in this section [11, 12]. The result for the energy collimation extracted from YaJEM+BW (21) will be compared with the medium-modified NLLA and LLA formulæ (15). The medium modification parameter f_{med} is set to its mean value $\langle f \rangle_{med} = 0.4$, obtained from averaging over the hydrodynamical model. The result of the numerical inversion of (15) and (16) will be displayed in the form given by (24) in both cases.

3.3 Medium-modified jet energy collimation in gluon jets

In table 2, we display gluon dijets at three different center of mass energies $\sqrt{s} = 150 - 500$ GeV, which are reconstructed by using the anti-k_t algorithm [24, 25] for the radii $R = 1$ and $R = 0.3$. As described above, E_{rec} is the recovered jet energy of the leading parton $E_{rec} = \hat{z}\sqrt{s}/2$ inside the cone R and Q is the jet virtuality. We can see that gluon jets carry the energy fractions $\hat{z} \sim 4/5$ and $2/3$

$\sqrt{s}$ (GeV)	R	E_{rec} (GeV)	Q (GeV)	R	E_{rec} (GeV)	Q (GeV)
150	1.0	64.8	64.8	0.3	46.3	13.8
300	1.0	131.3	131.3	0.3	98.0	29.4
500	1.0	220.4	220.4	0.3	168.9	50.7

Table 2: Reconstructed jet energies inside the cone radii $R = 1.0$ and $R = 0.3$.

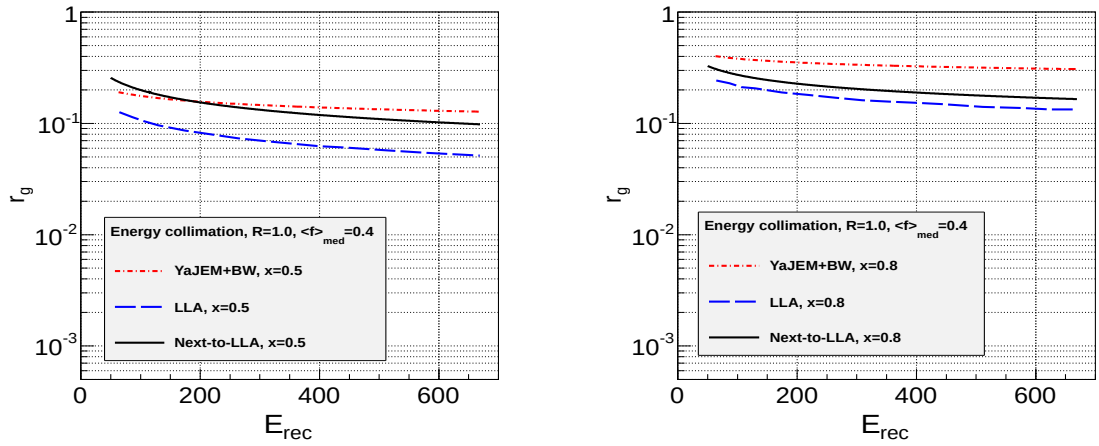

Figure 3: Energy collimation inside a gluon jet for $x = 0.5$ (left) and $x = 0.8$ (right) with $R = 1.0$.

of the leading parton for $R = 1.0$ and $R = 0.3$ respectively. Indeed, $\sqrt{s}/2$ is the energy of the leading parton spread in the whole hemisphere and $\sqrt{s}/2 - E_{rec}$ is that part of the jet energy that is lost outside R, which should not be confused with the jet energy inside the cone shell $r \leq r' \leq R$. We can see

that the correlation between parton kinematics and reconstructed jet kinematics gets increasingly blurred for small reconstruction radii. Thus, the choice $R = 0.3$ used by the CMS experiment provides a more severely biased jet energy.

In Fig.3, we display the energy collimation at $R = 1.0$ in gluon jets:

$$r_g = R\left(\frac{Q}{\Lambda_{\rm QCD}}\right)^{-\gamma_g(x,N_s)} \tag{25}$$

in the energy range $60 \leq E_{rec}(\text{GeV}) \leq 600$ for RHIC and LHC phenomenology. We choose the energy fractions $x = 0.5$, $x = 0.8$ and compare the NLLA prediction (15) with the LLA (16) and YaJEM+BW (21) for $\langle f\rangle_{med} = 0.4$. The disagreement between the LLA prediction and YaJEM+BW is quite substantial and mainly due to the lack of other perturbative contributions in this calculation, whereas the NLLA prediction improves the agreement. As expected for $x = 0.5$, the $\mathcal{O}(\alpha_s)$ correction in the NLLA formula (15) proves to be larger than for $x = 0.8$. The shape of the energy collimation provided by the NLLA (15) and the LLA (16) are identical but steeper than the slope of the energy collimation provided by YaJEM+BW. Therefore, the NLLA and LLA predictions overestimate the energy collimation compared to the YaJEM+BW prescription.

Decreasing the jet radius to the value used by the CMS experiment at 2.76 TeV PbPb collisions $R = 0.3$ leads to a sizable hardening of the biased jet which may provide a better comparison between the NLLA, LLA and YaJEM+BW predictions for the jet energy collimation. The bias drives results to a generic outcome, so differences in the comparison must disappear as the bias gets stronger. That is why, in Fig.4 we display the same curves as in Fig. 3 for $R = 0.3$. We can see that the description provided by the NLLA (21), LLA (16) and YaJEM+BW (21) calculations are in better agreement with each other than the results displayed in Fig. 3 for $R = 1.0$. As expected, in the LLA, NLLA and YaJEM+BW computations, the energy collimation is stronger as the jet energy increases.

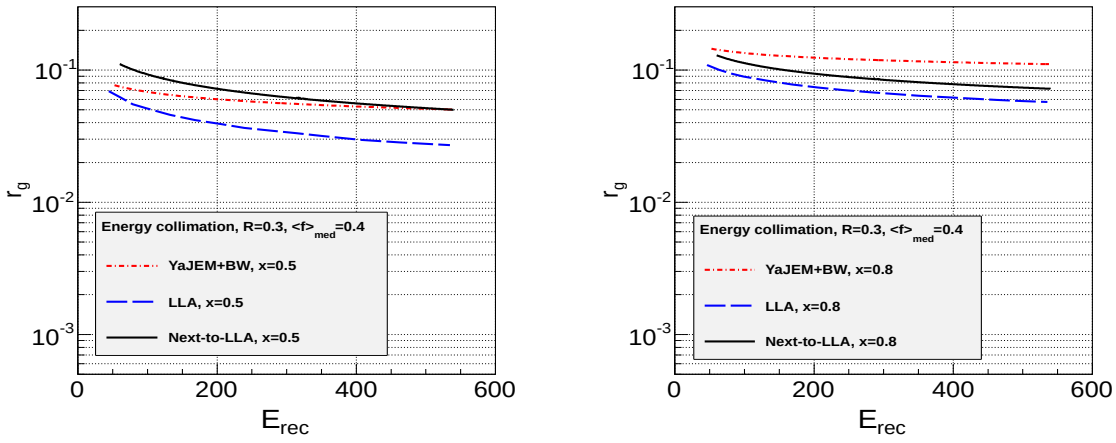

Figure 4: Collimation of energy inside a gluon jet for $x = 0.5$ (left) and $x = 0.8$ (right) with $R = 0.3$.

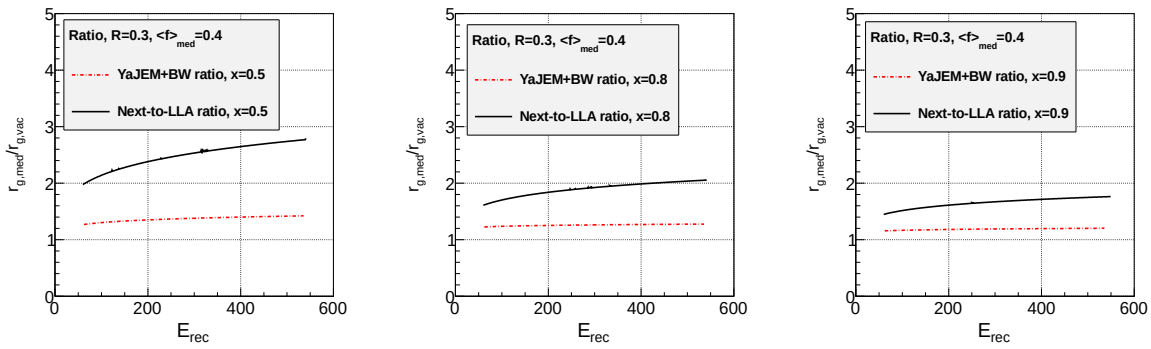

Figure 5: Medium-modified and vacuum energy collimation ratios $r_{g,med}/r_{g,vac}$ for $x = 0.5$ (left), $x = 0.8$ (center) and $x = 0.9$ (right) with $R = 0.3$.

As a consequence of jet quenching in high energy heavy-ion collisions, medium-modified showers are expected to broaden compared with vacuum showers. This effect can be quantified via the shower energy collimation by taking the ratios $r_{g,med}/r_{g,vac}$ with $\langle f \rangle_{med} = 0.4$ for the medium in the numerator and $\langle f \rangle_{med} = 0$ for vacuum in the denominator with the NLLA formula (15) and the YaJEM analysis (21). The ratios are displayed in Fig. 5 for the energy fractions $x = 0.5, 0.8, 0.9$ and the jet radius $R = 0.3$. For $x = 0.5$, the NLLA formula predicts a twice higher sub-jet broadening (i.e. smaller energy collimation) than YaJEM+BW, while for $x = 0.8 - 0.9$ the agreement is improved but still different by a factor of $\sim 1.5 - 1.2$, reaching the best agreement for $x = 0.9$. Thus, as the energy fraction x increases, the jet broadening inside the smaller cone r decreases. As expected, the NLLA correction seems to play a more important role as x decreases. The last can be observed in Fig. 5 as one compares the shapes of the NLLA prediction with YaJEM+BW. The YaJEM+BW prediction tends to flatten while the NLLA formula increases, making the vertical difference higher as the energy scale increases.

3.4 Medium-modified jet energy collimation in quark jets

In table 3, we display quark di-jets for the same values of center of mass energy and R. We can see that the recovered jet energy slightly increases compared with that displayed in table 2 for gluon jets. The

$\sqrt{s}$ (GeV)	R	E_{rec} (GeV)	Q (GeV)	R	E_{rec} (GeV)	Q (GeV)
150	1.0	70.0	70.0	0.3	58.5	17.6
300	1.0	141.0	141.0	0.3	100.1	30.0
500	1.0	236.0	236.0	0.3	205.9	61.5

Table 3: Reconstructed jet energies inside the cone radii $R = 1.0$ and $R = 0.3$.

energy collimation inside a quark jets (17) can be rewritten in the form,

$$r_q = R\left(\frac{Q}{\Lambda_{\rm QCD}}\right)^{-\gamma_q(x,N_s)}. \tag{26}$$

Accordingly, in Fig.6 and Fig.7, we display the quark jet energy collimation for the energy fractions $x = 0.5$ and $x = 0.8$ by the sub-jet with the medium modification value $\langle f\rangle_{med} = 0.4$. As for

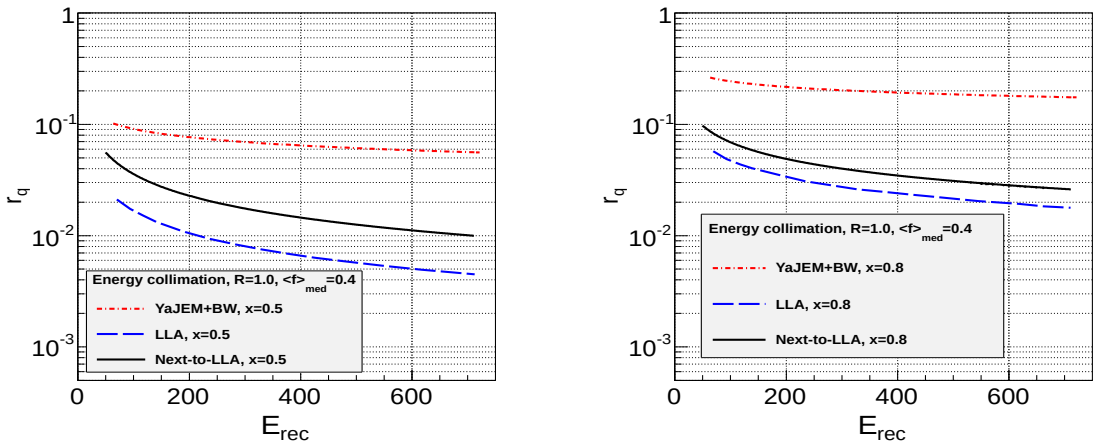

Figure 6: Collimation of energy inside a gluon jet for $x = 0.5$ (left) and $x = 0.8$ (right) with $R = 1.0$.

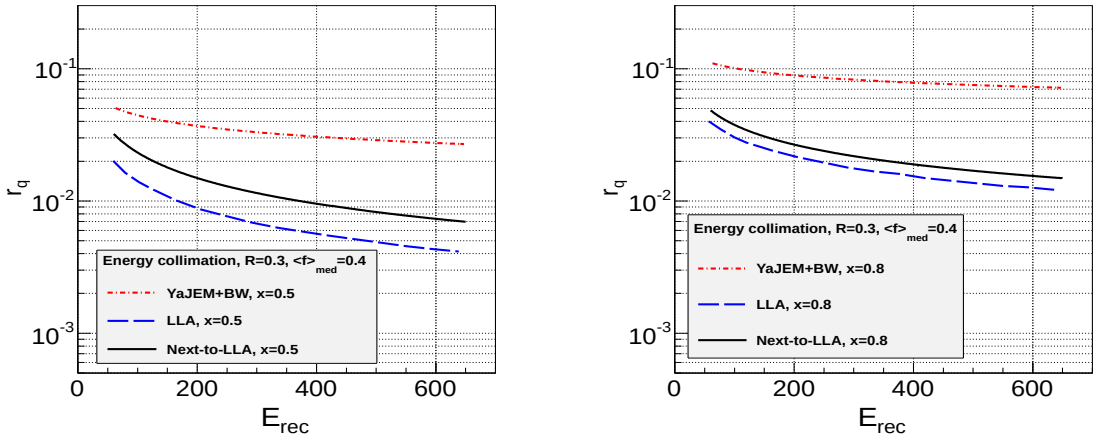

Figure 7: Collimation of energy inside a quark jet for $x = 0.4$ (left) and $x = 0.8$ (right) with $R = 0.3$.

gluon jets, our predictions are in better agreement with YaJEM+BW for $R = 0.3$ than for $R = 1.0$. For $R = 1.0$, the NLLA predictions underestimate YaJEM+BW for $x = 0.5$ and $x = 0.8$. However, for $R = 0.3$, the disagreement is reduced as for gluon jets. Furthermore, the correction due to the shift in $\ln x$ is smaller in a quark jet compared to a gluon jet and LLA predictions in gluon jets are in better agreement

with YaJEM+BW than in quark jets. The last statements suggest that NLLA and LLA predictions should be in better agreement with YaJEM+BW for much harder jets, i.e. $R = 0.1$ as displayed in Fig. 8. The study of smaller jet resolutions such as $R = 0.1$ which further biases QCD showers, is shown to

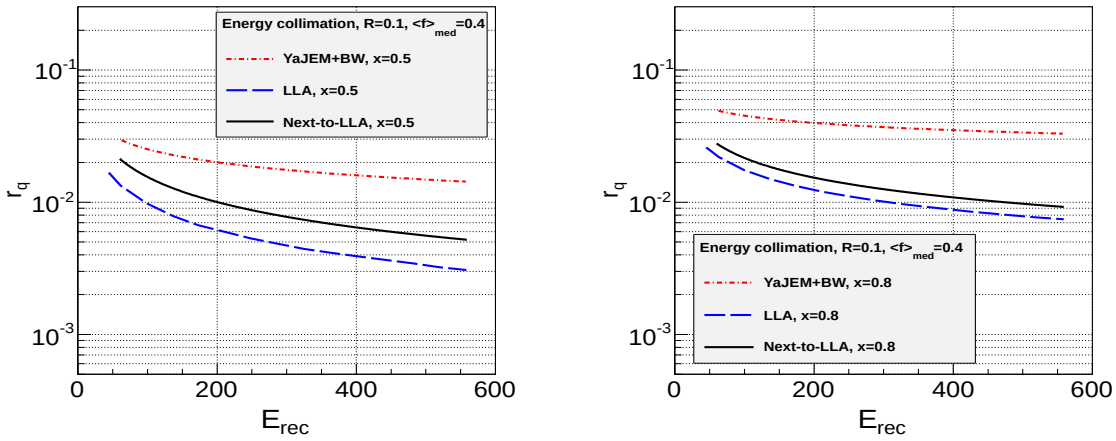

Figure 8: Collimation of energy inside a gluon jet for $x = 0.5$ (left) and $x = 0.8$ (right) with $R = 0.1$.

always improve quark/gluon tagging at the LHC [39]. In Fig. 9, we display the ratios $r_{q,med}/r_{q,vac}$ of

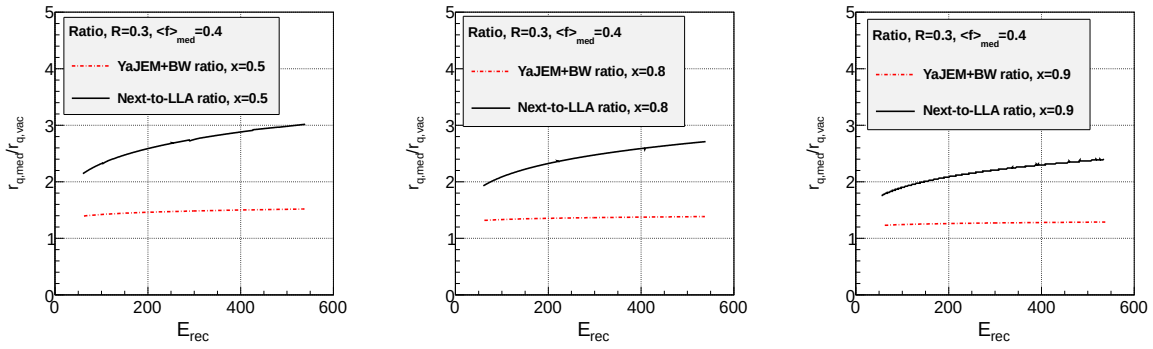

Figure 9: Medium-modified and vacuum energy collimation ratios $r_{q,med}/r_{q,vac}$ for $x = 0.5$ (left), $x = 0.8$ (center) and $x = 0.9$ (right) with $R = 0.3$.

the energy collimation in the medium and the vacuum. The results clearly show the quark jet broadening as a consequence of jet quenching. The comparison between the NLLA and LLA predictions is worse than for gluon jets.

In table 4, we present the values of the slopes $\gamma_A(x, N_s)$ provided by YaJEM+BW ($\langle f \rangle_{med} = 1.4$) and Pythia 6. As displayed in the above figures for the energy collimation, the values are smaller than in the NLLA and LLA calculations presented in table 1. However, the trends shown by the variation of $\gamma_A(x, N_s)$ as a function of x and N_s are similar ($\gamma_q > \gamma_g$). In particular, the slopes decrease as the energy

fraction decreases for a given value of N_s. For a fixed value of x, the energy collimation flattens as N_s increases. We can see that our calculations and YaJEM+BW predict a much stronger energy collimation

YaJEM+BW	$x = 0.5$	$x = 0.8$	Pythia 6	$x = 0.5$	$x = 0.8$
$\gamma_g(x, 1.4)$	0.17	0.11	$\gamma_g(x, 1)$	0.21	0.14
$\gamma_q(x, 1.4)$	0.24	0.17	$\gamma_q(x, 1)$	0.29	0.20

Table 4: YaJEM+BW values of the slope $\gamma_A(x, N_s)$ of the energy collimation for $N_s = 1.4$ (medium) and Pythia 6 values for $N_s = 1$ (vacuum).

in a quark jets than in gluon jets. Physically, this is because gluon jets have a color charge roughly twice bigger $N_c/C_F = 9/4$ than quark jets, or equivalently, gluon jet multiplicities are higher than quark jet multiplicities by the same factor asymptotically [40]. Moreover, the first splitting dominates the jet width, which for quark jets only has the available splitting $q \to qg$ where the emitted gluon is preferentially soft and does not alter the transverse jet shape, whereas gluon jets can split into $g \to q\bar{q}$ pairs where both quarks tend to be equally hard, which can widen the shape substantially. In both YaJEM+BW and the calculation, the energy collimation is hence steeper for quark jets than for gluon jets.

Equations (15) and (16) provide a simple description of the jet energy collimation under consideration and can not be in perfect agreement with the YaJEM+BW description. The last suggests that other perturbative contributions arising from the splittings $q \to qg$ and $g \to q\bar{q}$ should be included in (1) in the form $D_q(x, E\Theta_0, xE\Theta) = D_q^q(x, E\Theta_0, xE\Theta) + D_q^g(x, E\Theta_0, xE\Theta)$ for quark jets and $D_g(x, E\Theta_0, xE\Theta) = D_g^g(x, E\Theta_0, xE\Theta) + D_g^q(x, E\Theta_0, xE\Theta)$ for gluon jets, with the full resummed contribution of the soft-collinear logarithms in DGLAP FFs [28, 29]. Indeed, as the jet energy increases, the contributions from the double logarithmic contributions $\alpha_s \frac{dz}{z} \frac{d\Theta}{\Theta}$ ($z = E_g/E$) increase asymptotically, that may explain why the difference between YaJEM+BW and the NLLA predictions gets wider as the jet energy E increases. Moreover, the more accurate treatment of phase space in both Pythia and YaJEM have not been taken into account in the NLLA and LLA calculations.

3.5 Hadronization effects in the energy collimation

In Fig. 10 we display the energy collimation inside gluon and quark jets in the vacuum using Pythia 6. The role of hadronization is displayed by comparing the energy collimation for final state hadrons and final state partons clustered inside the radius $R = 0.3$ in the energy range $50 \leq E_{rec}(\mathrm{GeV}) \leq 700$ by using the anti-k_t algorithm [24, 25]. The hadronic energy collimation has been labeled as "Pythia 6" and the partonic energy collimation, "Pythia 6 parton shower". Since the hadronization is modeled to occur outside the medium, we limited the comparison to Pythia 6 since the results would be identical for YaJEM+BW with a slightly larger normalization (see figures 4 and 7 for comparison) as a consequence of the jet broadening. As we can see, the hadronization biases the partonic energy collimation for jet energies < 400 GeV but this effect is $\sim 5\%$ at RHIC energy scales and smaller than 1% at LHC energy scales. For jet energies > 400 GeV the role of hadronization becomes negligible and therefore irrelevant

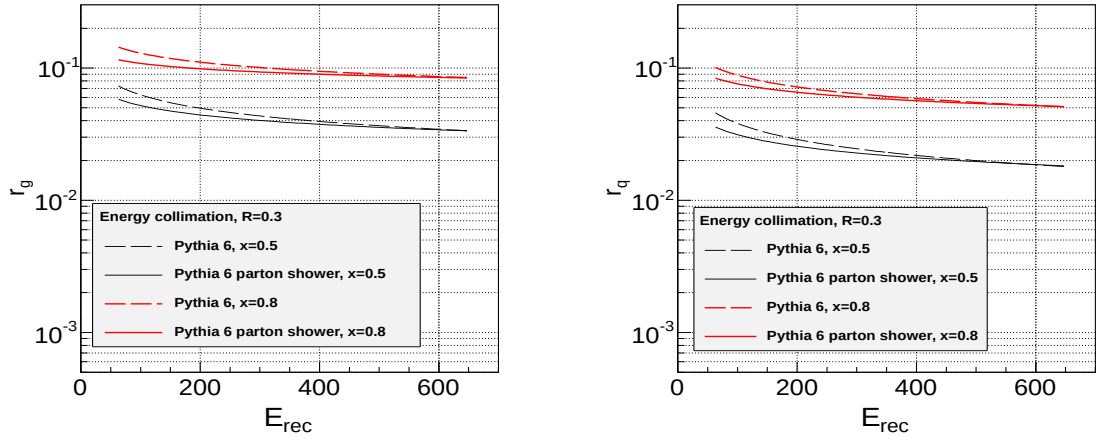

Figure 10: Parton versus hadron energy collimation for $x = 0.5$ and $x = 0.8$ inside a gluon jet (left) and a quark jet (right) with $R = 0.3$.

for the study of this observable. In general hadronic shower are less collimated than a fictitious parton shower at small energy scales.

4 Jet shape: comparison with PbPb CMS data

The integrated jet shape $\Psi(r; R)$ measures the fraction of the jet energy of size R contained in a sub-cone of size r such that $\Psi(R; R) = 1$. The differential jet shape reads [22],

$$r\psi(r; R) = r\frac{d\Psi}{dr},$$

where

$$\frac{d\Psi}{dr} = \frac{1}{E_{rec}} \int de\, e \frac{d^2N}{dedr'}, \quad E_{\rm rec} = \int_0^R dr' \int de\, e \frac{d^2N}{dedr'}. \tag{27}$$

Hence, the integration of (27) leads to the expression written in (21) for the energy fraction x used in the framework of the energy collimation, which will be identified with the integrated jet shape hereafter: $x \equiv \Psi(r; R)$. Our NLLA and LLA predictions for the integrated jet shape will be therefore based on the maximal angular aperture $\Theta \equiv r$ where the bulk of the jet energy is contained, as we discussed in section 2.1.

For the computation of the integrated jet shapes extracted from (27), we will limit our study to charged particles only inside the clustering radius $R = 0.3$ used by the CMS experiment [7]. The initial distribution of gluons and quarks initiated showers in this section is determined by the convolution of PDFs and nPDFs with the LO matrix elements of the final cross-section at the given hard factorization scale of the process. The LO matrix elements of the partonic cross-section can be computed analytically [41]. PDFs and nPDFs are provided by the CTEQ [37] and EKS [38] for pp and PbPb collisions in the vacuum and the medium respectively. The analysis carried out for the jet shapes is hence different compared with the

analysis for the energy collimation in subsections 3.3 and 3.4 where the center of mass energy of the hard parton system was fixed to a certain value $\sqrt{s}$. A large number of quark and gluon dijets are randomly generated based in the pQCD spectrum inside the energy range $200 \leq \sqrt{s}(\mathrm{GeV}) \leq 600$ and clustered by using the anti-k_t algorithm with $R = 0.3$. After clustering all charged hadrons with $e > 1$ GeV inside the given cone $R = 0.3$, jet energies E_{rec} are required to fulfill CMS trigger conditions imposed by the restriction $E_{\mathrm{rec,jet}} \geq 100$ GeV. The requirement imposed by the trigger selection in the analysis will be referred to as biased shower, while that including all clustered jet energies will be referred to as unbiased shower in the following. Accordingly, the fraction of gluon jets in one sample is biased by the trigger condition from $f_g^{vac} \approx 0.4$ in the unbiased case to $f_g^{vac} \approx 0.2$ in the biased case in vacuum showers; and from $f_g^{med} \approx 0.3$ to $f_g^{med} \approx 0.1$ in medium showers. Thus, quark jets are dominant in the analysis and particularly in the medium. The fraction of gluon jets in a sample is used for the computation of the

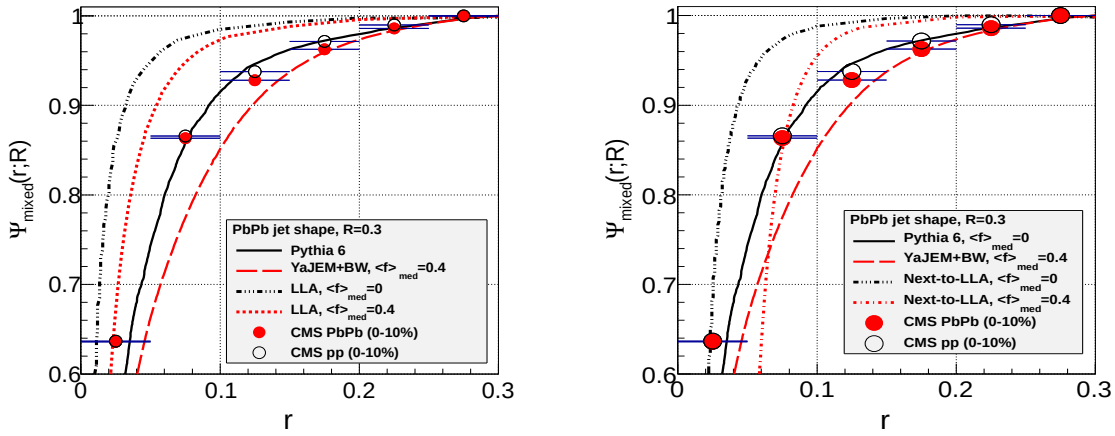

Figure 11: Jet shape for CMS pp and $PbPb$ data with $R = 0.3$, compared with Pythia 6, YaJEM+BW, LLA formula (left panel) and NLLA formula (right panel).

mixed integrated jet shape given by the linear combination for gluon and quark jets in the form:

$$\Psi_{\mathrm{mixed}}(r;R) = f_g \Psi_g(r;R) + (1 - f_g)\Psi_q(r;R) \tag{28}$$

for direct comparison of LLA (16), NLLA (15), Pythia 6 and YaJEM+BW with CMS data. For the LLA and NLLA predictions in the vacuum we set $\langle f \rangle_{med} = 0$ and in the medium $\langle f \rangle_{med} = 0.4$. In YaJEM+BW, f_{med} is computed event by event as described in section 3.1. Instead of treating quark and gluon jets independently in this framework, it is more straightforward to mix the differential distributions for the energy flux (27) and compare with the mixed jet shape from Pythia and YaJEM+BW with account of hadronization. By doing so, all jets cluster to the biased mean jet energy value $E_{rec} \sim 140$ GeV that will be used as energy input for the NLLA and LLA calculations. In Fig. 11, we show the LLA, Pythia 6 and YaJEM+BW for $\langle f \rangle_{med} = 0.4$ jet shapes compared with pp and PbPb CMS data in the left panel, the NLLA, Pythia 6 and YaJEM+BW jet shapes for $\langle f \rangle_{med} = 0.4$ compared with pp and PbPb CMS data in the right panel. We can see that the LLA and NLLA qualitatively describe the features of the jet shapes in

both vacuum and medium but an important disagreement persists. Compared to the LLA calculation, the NLLA approaches the data as the the jet shape decreases and particularly for more collimated sub-jets r, as expected. Translating this statement to the energy collimation, we show the NLLA correction to widen the energy dependence of r and to increase the difference with the LLA calculation as the sub-jet energy fraction (jet shape) decreases. Thus, though the NLLA and LLA predictions seem to capture the main ingredients of the hard fragmentation process in this framework, the account of all fragmentation probabilities, mainly those containing soft gluon contributions should be taken into account in a more accurate theoretical framework. Pythia 6 provides instead a good agreement with pp CMS data for biased jets. YaJEM+BW describes the shower medium modifications by reproducing the jet broadening at slightly larger values of r to the right, as the medium-modified NLLA and LLA jet shapes. Though the YaJEM+BW calculation does not reproduce the data points exactly, the curve fits the systematic error bars of the CMS PbPb data. As observed, the sub-jet broadening shown by the data is very small but in better agreement with the sub-jet broadening shown by the Monte Carlos than with that shown by the theoretical calculations with the BW prescription.

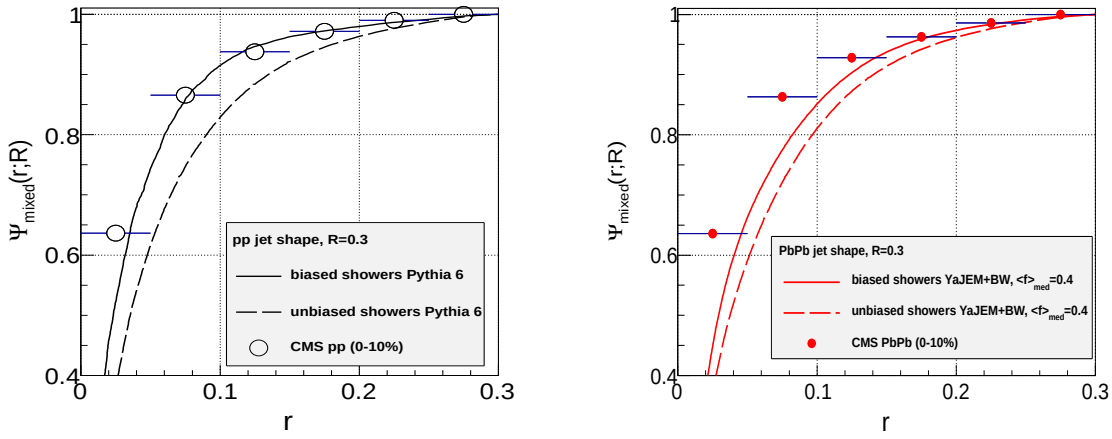

Figure 12: Biased versus unbiased jet shape for CMS pp data (left panel) and PbPb data (right panel) with $R = 0.3$.

In Fig. 12 we compare the biased ($E_{rec,jet} \geq 100$) GeV and unbiased (all jets) cases obtained with Pythia 6 and YaJEM+BW with pp (left panel) and PbPb (right panel) CMS data. As can be seen, the shower structure is affected by imposing a jet energy condition which leads to a better agreement between the biased jet shape and the data than the unbiased jet shape.

4.1 Hadronization effects in gluon and quark jet shapes

Finally, in Fig. 13, we display the jet shape obtained with Pythia 6 for a jet energy ~ 110 GeV and display the role of hadronization between a fictitious partonic shower and a hadronic shower. For the hadronic shower the study includes all particles in an event. The shift due to the role of hadronization

is very small and can be cross-checked to be the same as the shift displayed for the energy collimation at $E_{rec} \sim 110$ GeV in Fig. 10. However, for energy scales slower than 400 GeV, the partonic jet shape obtained from Pythia 6 is slightly closer to the theoretical calculations. From the comparison displayed in Fig. 10 we can conclude that for high energy jets the shift between both curves is very small and vanishes asymptotically. This is another part of the reason why, Pythia 6 and YaJEM+BW with account of hadronization provide a more accurate agreement with the data.

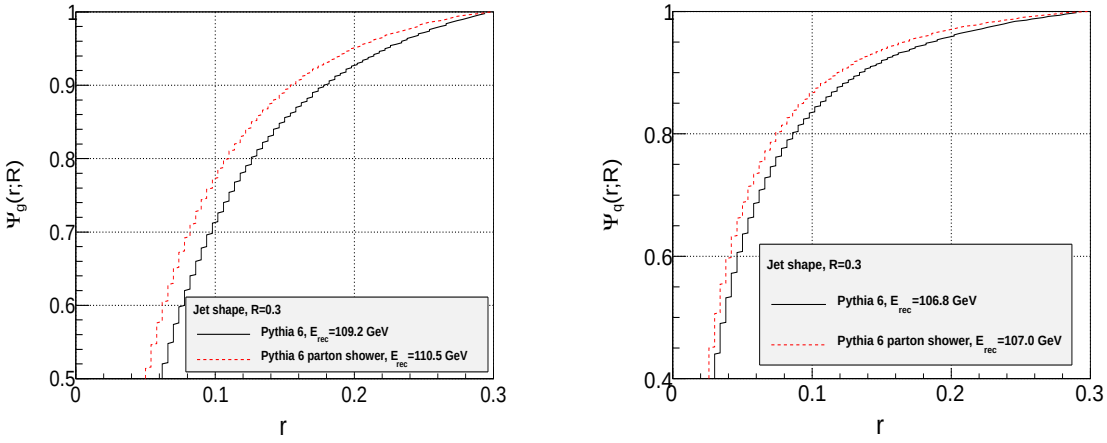

Figure 13: Parton versus hadron jet shape inside a gluon jet (left) and a quark jet (right) with $R = 0.3$.

5 Summary

In the paper, we studied the energy collimation of gluon and quark jets produced in heavy-ion collisions and the jet shape of hadrons produced in pp and PbPb collisions at 2.76 GeV. The NLLA energy collimation seems to capture a more complete analytical description of this observable than the LLA energy collimation obtained in [20], particularly in gluon jets, but a disagreement with YaJEM+BW and the data still persists, which is more pronounced in more biased quark showers with smaller jet resolutions, i.e. $R = 0.1$. The difference between gluon and quark jets for this observable is well qualitatively described by both medium-modified NLLA and YaJEM+BW descriptions, i.e. both provide stronger energy collimation in quark jets than in gluon jets and the NLLA description improves the normalization for partons carrying the intermediate energy fractions $x \sim 0.5$. Though this quantity can not be directly measured for each type of jet separately, their combination would lead to the quantification of the jet broadening at high energy heavy-ion experiments, i.e. the NLLA formula in the vacuum ($N_s = 1$) and Pythia 6 predict a much faster increase of the energy collimation than the medium-modified NLLA ($N_s = 1.4$) and YaJEM+BW calculations as the energy scale increases.

We extracted the jet shape from the analysis performed for the energy collimation and compared the NLLA, LLA, Pythia 6 and YaJEM+BW predictions with the CMS pp and PbPb data at 2.76 TeV. The

final biased and unbiased comparison for this observable clearly shows the importance of taking all jet finding conditions into account in order to get as much accurate results as possible in the comparison of Monte Carlo event generators and theoretical predictions with the data.

The NLLA and LLA predictions qualitatively describe the jet shapes but fail to reproduce the right normalization of this observable. The reasons for this disagreement are the same as those previously presented for the energy collimation in the last paragraph of subsection 3.4. The biased jet shape provided by Pythia 6 is in very good agreement with pp CMS data and the medium-modified biased jet shape from YaJEM+BW qualitatively describes the sub-jet broadening shown by PbPb CMS data for larger values of r, although it is much weaker in CMS data than in the YaJEM+BW result. Gluon jets produce a wider shower brodening than quark jets but they get even more suppressed by biases than quark jets, which clearly dominate the data for $E_{rec,jet} \geq 100$ GeV. This new example proves that biases appear to strongly suppress the relevant physics of jet quenching we want to understand and hence, information is lost concerning the early stage of jet evolution and its interaction with the medium in the study of this observable.

Of course our results for the jet shape and comparison with the data reflect the characteristics of the BW prescription and hence should be compared and improved with calculations using other models; a comparison with YaJEM-DE [42] may for instance be desirable.

Acknowledgements

R. Pérez-Ramos is grateful to Beomsu Chang, DongJo Kim and Norbert Novitzky for their expert support on the Monte Carlo analysis and coding techniques, and to Wolfgang Ochs for useful discussions and comments on the manuscript. We acknowledge support from the Academy researcher program of the Academy of Finland, Project No. 130472.

References

[1] David d'Enterria. Jet quenching. 2009.

[2] Miklos Gyulassy and Xin-nian Wang. Multiple collisions and induced gluon Bremsstrahlung in QCD. Nucl.Phys., B420:583–614, 1994.

[3] R. Baier, Yuri L. Dokshitzer, Alfred H. Mueller, S. Peigne, and D. Schiff. Radiative energy loss and p(T) broadening of high-energy partons in nuclei. Nucl.Phys., B484:265–282, 1997.

[4] K. Adcox et al. Suppression of hadrons with large transverse momentum in central Au + Au collisions at $\sqrt{s}$ = 130 GeV. Phys. Rev. Lett., 88:022301, 2002.

[5] Stephen Scott Adler et al. Absence of suppression in particle production at large transverse momentum in s(NN)**(1/2) = 200-GeV d + Au collisions. Phys. Rev. Lett., 91:072303, 2003.

[6] A. Adare et al. Onset of pi0 Suppression Studied in Cu+Cu Collisions at sNN=22.4, 62.4, and 200 GeV. Phys.Rev.Lett., 101:162301, 2008.

[7] Serguei Chatrchyan et al. Modification of jet shapes in PbPb collisions at $\sqrt{s_{NN}}$ = 2.76 TeV. 2013.

[8] Yuri L. Dokshitzer. Calculation of the Structure Functions for Deep Inelastic Scattering and e+ e- Annihilation by Perturbation Theory in Quantum Chromodynamics. (In Russian). Sov. Phys. JETP, 46:641–653, 1977.

[9] V. N. Gribov and L. N. Lipatov. Deep inelastic e p scattering in perturbation theory. Sov. J. Nucl. Phys., 15:438–450, 1972.

[10] Guido Altarelli and G. Parisi. Asymptotic Freedom in Parton Language. Nucl. Phys., B126:298, 1977.

[11] Mats Bengtsson and Torbjorn Sjostrand. Coherent Parton Showers Versus Matrix Elements: Implications of PETRA - PEP Data. Phys.Lett., B185:435, 1987.

[12] E. Norrbin and T. Sjostrand. QCD radiation off heavy particles. Nucl.Phys., B603:297–342, 2001.

[13] R. Baier, D. Schiff, and B. G. Zakharov. Energy loss in perturbative QCD. Ann. Rev. Nucl. Part. Sci., 50:37–69, 2000.

[14] Maya Shimomura. High-p(T) pi0, eta, identified and inclusive charged hadron spectra from PHENIX. Nucl.Phys., A774:457–460, 2006.

[15] S. Afanasiev et al. High-pT pi0 Production with Respect to the Reaction Plane in Au + Au Collisions at s(NN)**(1/2) = 200-GeV. Phys.Rev., C80:054907, 2009.

[16] Dan Magestro. Direct observation of dijets in central Au+Au collisions with STAR. Nucl.Phys., A774:573–576, 2006.

[17] J. Adams et al. Direct observation of dijets in central Au+Au collisions at s(NN)**(1/2) = 200-GeV. Phys.Rev.Lett., 97:162301, 2006.

[18] Nicolas Borghini and Urs Achim Wiedemann. Distorting the hump-backed plateau of jets with dense QCD matter. 2005.

[19] Yuri L. Dokshitzer, Valery A. Khoze, and S.I. Troian. Inclusive particle spectra from QCD cascades. Int. J. Mod. Phys., A7:1875–1906, 1992.

[20] Redamy Perez-Ramos and Vincent Mathieu. Collimation of energy in medium-modified QCD jets. Phys.Lett., B718:1421–1424, 2013.

[21] Thorsten Renk. Parton shower evolution in a 3-d hydrodynamical medium. Phys.Rev., C78:034908, 2008.

[22] M.H. Seymour. Jet shapes in hadron collisions: Higher orders, resummation and hadronization. Nucl.Phys., B513:269–300, 1998.

[23] Ivan Vitev, Simon Wicks, and Ben-Wei Zhang. A Theory of jet shapes and cross sections: From hadrons to nuclei. JHEP, 0811:093, 2008.

[24] Matteo Cacciari, Gavin P. Salam, and Gregory Soyez. FastJet User Manual. Eur.Phys.J., C72:1896, 2012.

[25] Matteo Cacciari and Gavin P. Salam. Dispelling the N^3 myth for the k_t jet-finder. Phys.Lett., B641:57–61, 2006.

[26] Yuri L. Dokshitzer, Dmitri Diakonov, and S. I. Troian. Hard Processes in Quantum Chromodynamics. Phys. Rept., 58:269–395, 1980.

[27] Yuri L. Dokshitzer, Valery A. Khoze, Alfred H. Mueller, and S. I. Troian. Basics of perturbative qcd. Gif-sur-Yvette, France: Ed. Frontières (1991) 274 p. (Basics of); and Rev. Mod. Phys. **60** (1988) 373.

[28] S. Albino, B.A. Kniehl, G. Kramer, and W. Ochs. The Evolution of hadron spectra in the modified leading logarithm approximation. Eur. Phys. J., C36:49–56, 2004.

[29] S. Albino, B. A. Kniehl, and R. Perez-Ramos. Medium-modified DGLAP evolution of fragmentation functions from large to small x. Nucl. Phys., B819:306–318, 2009.

[30] W. Furmanski and R. Petronzio. Singlet Parton Densities Beyond Leading Order. Phys. Lett., B97:437, 1980.

[31] P. Nason and B.R. Webber. Scaling violation in e+ e- fragmentation functions: QCD evolution, hadronization and heavy quark mass effects. Nucl.Phys., B421:473–517, 1994.

[32] Thorsten Renk. A Comparison study of medium-modified QCD shower evolution scenarios. Phys.Rev., C79:054906, 2009.

[33] Thorsten Renk. Constraining the Physics of Jet Quenching. Phys.Rev., C85:044903, 2012.

[34] Thorsten Renk. Energy dependence of the dijet imbalance in Pb-Pb collisions at 2.76 ATeV. Phys.Rev., C86:061901, 2012.

[35] Thorsten Renk. Theoretical assessment of jet-hadron correlations. Phys.Rev., C87(2):024905, 2013.

[36] Thorsten Renk, Hannu Holopainen, Risto Paatelainen, and Kari J. Eskola. Systematics of the charged-hadron P_T spectrum and the nuclear suppression factor in heavy-ion collisions from $\sqrt{s} =$ 200 GeV to $\sqrt{s} = 2.76$ TeV. Phys.Rev., C84:014906, 2011.

[37] Hung-Liang Lai, Joey Huston, Zhao Li, Pavel Nadolsky, Jon Pumplin, et al. Uncertainty induced by QCD coupling in the CTEQ global analysis of parton distributions. Phys.Rev., D82:054021, 2010.

[38] K.J. Eskola, V.J. Kolhinen, and C.A. Salgado. The Scale dependent nuclear effects in parton distributions for practical applications. Eur.Phys.J., C9:61–68, 1999.

[39] Jason Gallicchio and Matthew D. Schwartz. Quark and Gluon Jet Substructure. JHEP, 1304:090, 2013.

[40] Alfred H. Mueller. Square Root of alpha (Q**2) Corrections to Particle Multiplicity Ratios in Gluon and Quark Jets. Nucl. Phys., B241:141, 1984.

[41] K.J. Eskola and H. Honkanen. A Perturbative QCD analysis of charged particle distributions in hadronic and nuclear collisions. Nucl.Phys., A713:167–187, 2003.

[42] Thorsten Renk. Using Hard Dihadron Correlations to constrain Elastic Energy Loss. Phys.Rev., C84:067902, 2011.